Steady-State Analysis of Dual Active Bridge Converter with Single Phase Shift and Dual Phase Shift Modulation

Deepak Chandra Pandey
Department of Electrical Engineering
NIT Rourkela
Rourkela, India
pandeydeepak597@gmail.com

Pradyumna Kumar Behera
Department of Electrical Engineering
NIT Rourkela
Rourkela, India
pkb.vssut14@gmail.com

Monalisa Pattnaik
Department of Electrical Engineering
NIT Rourkela
Rourkela, India
pattnaikm@nitrkl.ac.in

***Abstract*—In recent times, dual active bridge (DAB) converter topology has gained significant limelight as a power conditioning unit, especially for electric vehicle (EV) charging infrastructure and DC microgrids. This is mainly due to added advantage offered by DAB with respect to other converters i.e. isolated DC-DC power conversion along with bidirectional power flow capability. The power flow control using a DAB converter for any application is primarily dictated by the understanding of state-of-art of modulation strategies. In this context, this article illustrates the analysis of the converter at steady-state for single-phase shift (SPS) and dual-phase shift (DPS) modulation techniques. The phase displacement/shift patterns and their correlation with different electrical parameters are represented analytically as well as graphically. Open-loop simulation results for both strategies are showcased for a 1 kW, 48 V/300 V system in boost mode of operation. The nature of all the voltage and current waveforms presented are matching with the results available in previous literature. The system can be further investigated for closed-loop operation in microgrid and EV applications having bidirectional power flow capability.**

***Index Terms*—Dual active bridge converter, Dual-phase shift, Isolated converter, Single-phase shift modulation.**

I. Introduction

DIMINISHING fossil reserves, alarming environmental pollution, and accelerating energy demand are the major concerns globally, particularly for the power and transportation sector. The incorporation of renewable energy-powered microgrids and the utilization of electric vehicles can be promising solutions for these emerging issues. The rapid development of power electronic converters has paved the way for the large-scale deployment of efficient microgrids and EV charging stations. The DC-DC converter is the key component that is comprehensively used in these applications [1]. The converters must exhibit high power density and handle high power conveniently. Conventional DC-DC converters are mostly non-isolated that have safety issues during large power transfer [2]. The input and output terminals can be isolated by the transformer, thus fault on the output side does not get transferred to the input side. Also, a transformer can step-up or step-down the voltage according to the requirement. Converters like fly-back, forward, and push-pull have isolation

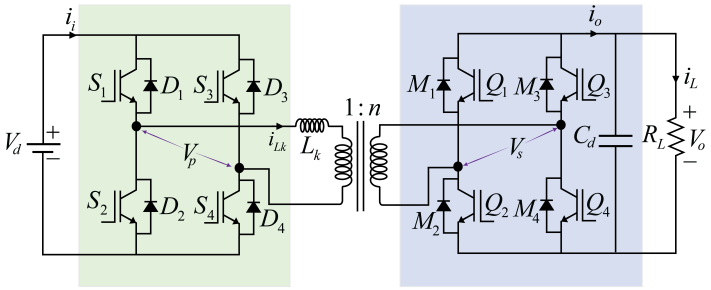

Fig. 1: Schematic of the DAB converter

but these converters do not allow bidirectional power flow which is one of the main requirements in EV and microgrid applications [3]. A dual active bridge (DAB) converter is one such which has advantages like galvanic isolation, bidirectional power flow capability, modular in nature, good parallelizability, and high efficiency. The architecture of DAB is simple, comprising two active bridges (i.e. primary and secondary) (Fig. 1). These two sides are isolated by a high-frequency intermediary transformer and the active power flow is enabled by the leakage inductance. The power transfer takes place through the converter only when there is a phase displacement among two square wave voltages present across the two active bridges. Over the years, different modulation methods have been developed to provide phase shifts, which has improved the performance of the converter as well. There are mainly four modulation techniques single phase shift (SPS), extended phase shift (EPS), dual-phase shift (DPS) and triple phase shift (TPS) modulation [4], [5]. Due to its advantages, research on DAB for different applications is still in progress. The use of DAB in a smart user network that is microgrid is discussed in [6], [7]. The electric vehicle has a battery charger based on DAB is given in [8], [9]. The application of DAB in a solid-state transformer (SST) for controlling the input current to the inverter with changes in traditional PI control is presented in [10]. The operation of DAB for PV application is discussed in [11].

In the SPS modulation method, the phase shift is given only between the corresponding switches of two active bridges having gate signals with 50% duty cycle. Thus, the voltage present at the transformer terminals is two level ac square wave and can be modified by adjusting the phase shift. The power flowing through the converter can be regulated by controlling the current passing through the inductor which depends on the voltage across the terminals of the transformer. SPS modulation is easy to implement and soft-switching can be achieved. However, it is not possible to realize zero voltage switching (ZVS) for the entire operating range. Extended phase shift modulation has two phase shifts [12]. One is present between the corresponding switches as in a single phase shift and the other is the inner phase shift present in one of the two active bridges only between the cross-connected switches. Due to the internal phase shift, the voltage at one side of the transformer is three-level and without the inner phase shift, it is two-level. This increases the soft-switching range whereas, to get reverse power flow inner phase shift is reversed. In comparison with EPS, DPS has an inner phase shift ratio between the cross-connected switches on both the active bridges along with the external phase shift as in SPS and the inner phase shift is equal on both sides [13]. Hence, the voltage is three-level on both sides of the transformer which further extends the ZVS range with increased efficiency. DPS is easier to implement with respect to EPS, as during reverse power flow inner phase shift side is not changed. TPS also has internal phase shift on both sides which is unequal [14]. Here also, three-level voltage is present across the primary and secondary winding. The above three modulation techniques can be called as special cases of TPS and are the most difficult to implement among the four. Though several articles have discussed the open-loop and closed-loop operation for various applications, still proper design and analysis of DAB with different modulation schemes are required to be investigated further to improve its performance and efficiency.

The steady-state operation for SPS modulation is described in the second section. The voltage and current equations for the different intervals are presented in this section. The third section includes the simulation results for both the SPS and DPS modulation techniques. Finally, the paper is concluded in section IV.

II. Steady State Analysis of DAB with SPS

In single phase shift modulation, the steady state operation of DAB can be segregated into four intervals based on the operation of switches [15]. Thus, the equation of voltage across and current through the inductor will also vary in the four intervals.

The voltage across the legs of the primary and secondary side bridges will be

$$V_p = V_d;\ V_s = V_o \tag{1}$$

Then, the secondary voltage referred to the primary side will be:

$$V_S' = -\frac{V_O}{n} = -V_O{}' \tag{2}$$

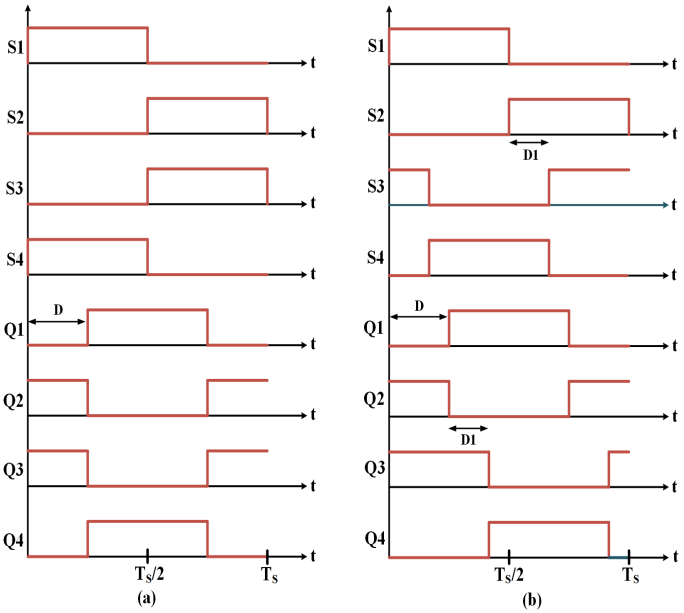

Fig. 2: Gate pulses for (a) SPS (b) DPS modulation schemes

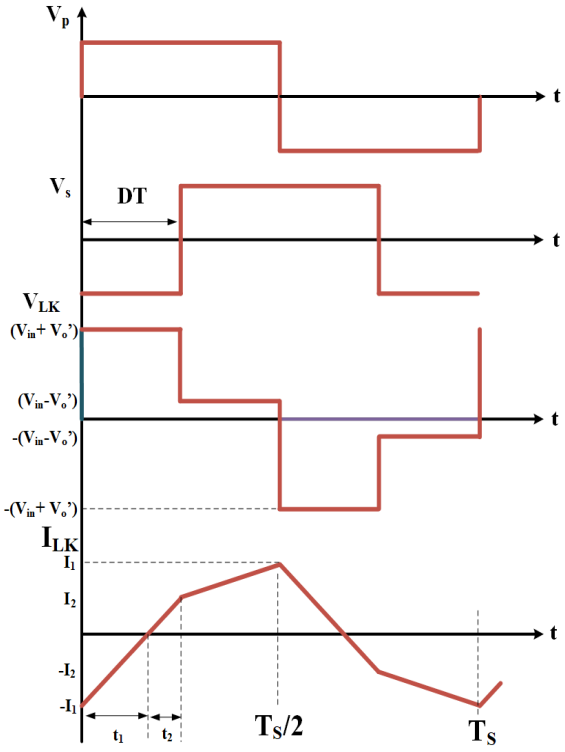

Fig. 3: Different voltages and inductor current waveforms of SPS scheme

Now, the voltage across the inductor and thus the current through the inductor will be given by:

$$V_{LK} = V_P - V_S' = V_d + V_O{}' \tag{3}$$

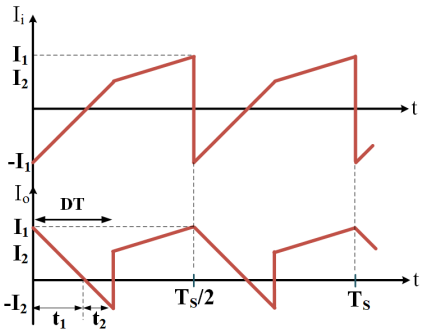

Fig. 4: Input current to the primary bridge and output current from the secondary bridge

The switches S_1 and S_4 of the primary bridge will continue to conduct, and gate pulses are given to switches Q_1 and Q_4 of the secondary bridge in the second interval. The voltages V_P, V_S and V_{LK} for this interval will be given by the following equations:

$$V_P = V_d;\ V_S' = V_O' \tag{4}$$

$$V_{LK} = V_d - V_O' \tag{5}$$

In the third interval, switches S_1 and S_4 of the primary bridge are turned off while S_2 and S_3 are switched on and Q_1 and Q_4 on the secondary bridge will continue to conduct. The voltages V_P, V_S', and V_{LK} for this interval are:

$$V_P = -V_d;\ V_S' = V_O' \tag{6}$$

$$V_{LK} = -\left(V_d + V_O'\right) \tag{7}$$

During the fourth interval, switches S_2 and S_3 are conducting on the primary bridge, and switches Q_2 and Q_3 start conducting now on the secondary side. The equation for the voltages are:

$$V_P = -V_d;\ V_S' = -V_O' \tag{8}$$

$$V_{LK} = -V_d + V_O' \tag{9}$$

Assuming V_P greater than V_S', the current through the inductor will rise or fall depending on the voltage across the inductor. Corresponding voltages V_P, V_S', V_{LK} and inductor current (I_{LK}) are shown in Fig. 3. Further, the input and output current can be written in terms of the inductor current for the four intervals are given below.

$$L\frac{di_{LK}}{dt} = V_{LK} = V_P - V_S' \tag{10}$$

Assuming the change in inductor current to be linear, in the first interval:

$$\frac{I_1 + I_2}{DT} = \frac{V_d + V_O'}{L} \tag{11}$$

Or

$$I_1 + I_2 = DT\frac{V_d + V_O'}{L} \tag{12}$$

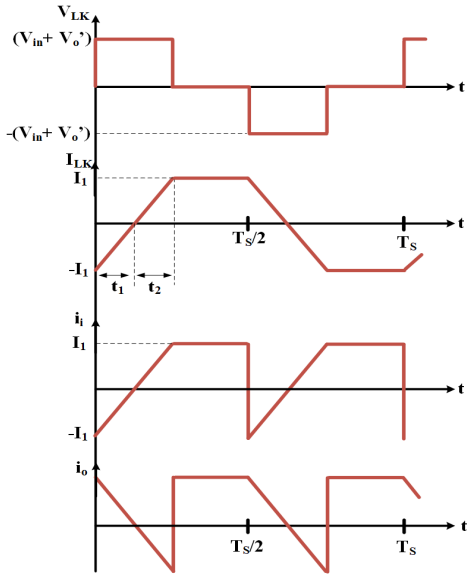

Fig. 5: Voltage and current for unity gain

Input and output currents are:

$$i_i = i_{LK};\ i_o = -i_{LK} \tag{13}$$

where, $T = \frac{T_s}{2}$, i_i = input current, i_o = output current. In the second interval:

$$\frac{I_1 - I_2}{(1-D)\,T} = \frac{V_d - V_O'}{L} \tag{14}$$

Or

$$I_1 - I_2 = (1-D)\,T\frac{V_d - V_O'}{L} \tag{15}$$

$$i_i = i_{LK} = i_o \tag{16}$$

The inductor current has half-wave symmetry, thus during the third and fourth interval it will be negative of the first and second interval. The input and the output current will be same as the first and second intervals, hence the frequency will be twice the switching frequency.

Now, adding (12) and (15)

$$I_1 = \frac{T}{2L}\left[V_d - V_O' + 2V_O'D\right] \tag{17}$$

And subtracting (12) and (15)

$$I_2 = \frac{T}{2L}\left[2V_dD - V_d + V_O'\right] \tag{18}$$

From the i_o waveform given in Fig. 4, it can be seen

$$\frac{I_1}{I_2} = \frac{t_1}{t_2} \tag{19}$$

and

$$t_1 + t_2 = DT \tag{20}$$

or

$$t_1 = \frac{DT}{1 + \frac{I_2}{I_1}} \tag{21}$$

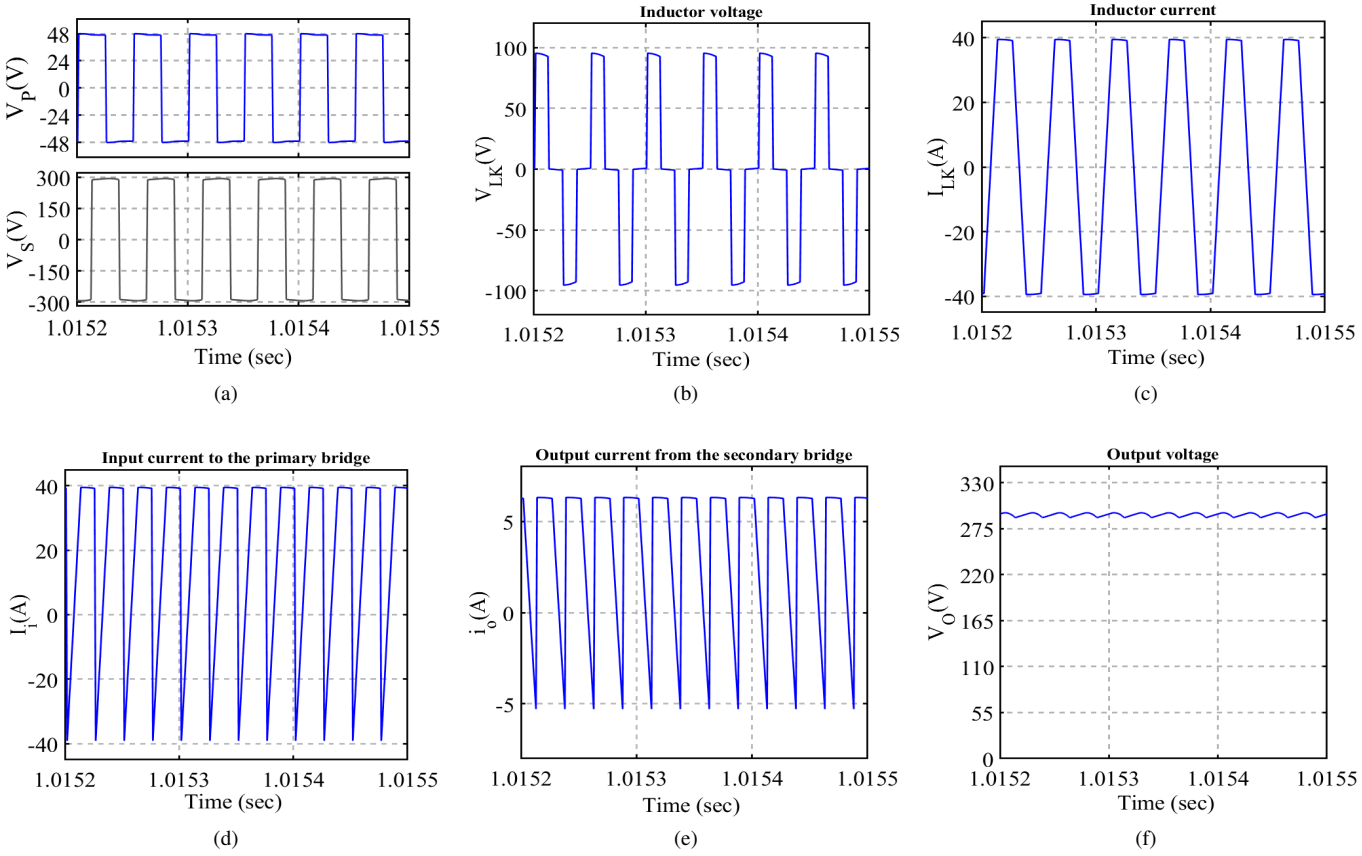

Fig. 6: Simulation results for SPS modulation (a) Primary and secondary voltage (b) Inductor voltage (c) Inductor current (d) Input current to the primary bridge (e) Output current from the secondary bridge (f) Output voltage

Putting I_1 and I_2 in (19) and (21)

$$t_1 = \frac{T}{2}\left[\frac{V_d - V_O{}' + 2V_O{}'D}{V_d + V_O{}'}\right] \tag{22}$$

$$t_2 = \frac{T}{2}\left[\frac{2V_dD - V_d + V_O{}'}{V_d + V_O{}'}\right] \tag{23}$$

Thus, the equation for average input and output current can be evaluated from Fig. 4 by taking the area under these waveforms:

$$I_i = \frac{(1-D)\,DTV_O}{L} \tag{24}$$

and

$$I_o = \frac{(1-D)\,DTV_d}{L} \tag{25}$$

Also, voltage gain can be evaluated as

$$G = \frac{V_O}{nV_d} = \frac{I_oR}{nV_d} = D\,(1-D)\,m \tag{26}$$

where, $m = \frac{TR}{Ln^2}$. For the case, when G = 1,

$$V_O{}' = V_d \tag{27}$$

Hence, solving equation (12), (15) and (27)

$$I_1 = I_2 = DT\frac{V_d + V_O{}'}{2L} \tag{28}$$

For this condition, the waveforms of inductor voltage, inductor current, input and output currents of both the bridges are shown in Fig. 5. Here, the rms and maximum value of inductor current are minimum, thus giving minimum conduction losses.

The equation for output power [16] is

$$P_o = V_oI_o = \frac{V_dV_OD(1-D)T_S}{2nfL} \tag{29}$$

III. Simulation Results of DAB

The simulation of the DAB converter with SPS and DPS modulation schemes is carried out in MATLAB/Simulink environment. The different parameters of DAB and high-frequency transformer for a 1 kW, 48 V/300 V system are presented in Table 1.

A. With SPS Modulation

The simulation results for the SPS modulation scheme are presented in Fig. 6. The phase shift of 25 % with respect to the time period is given between the two active bridges. The voltages across the primary, secondary bridges and inductor are shown in Fig. 6 (a) and (b) respectively. When the inductor voltage is positive, the inductor current rises and falls when it is negative correspondingly as shown in Fig. 6 (c). Based on the switching of the devices, the input and output current of

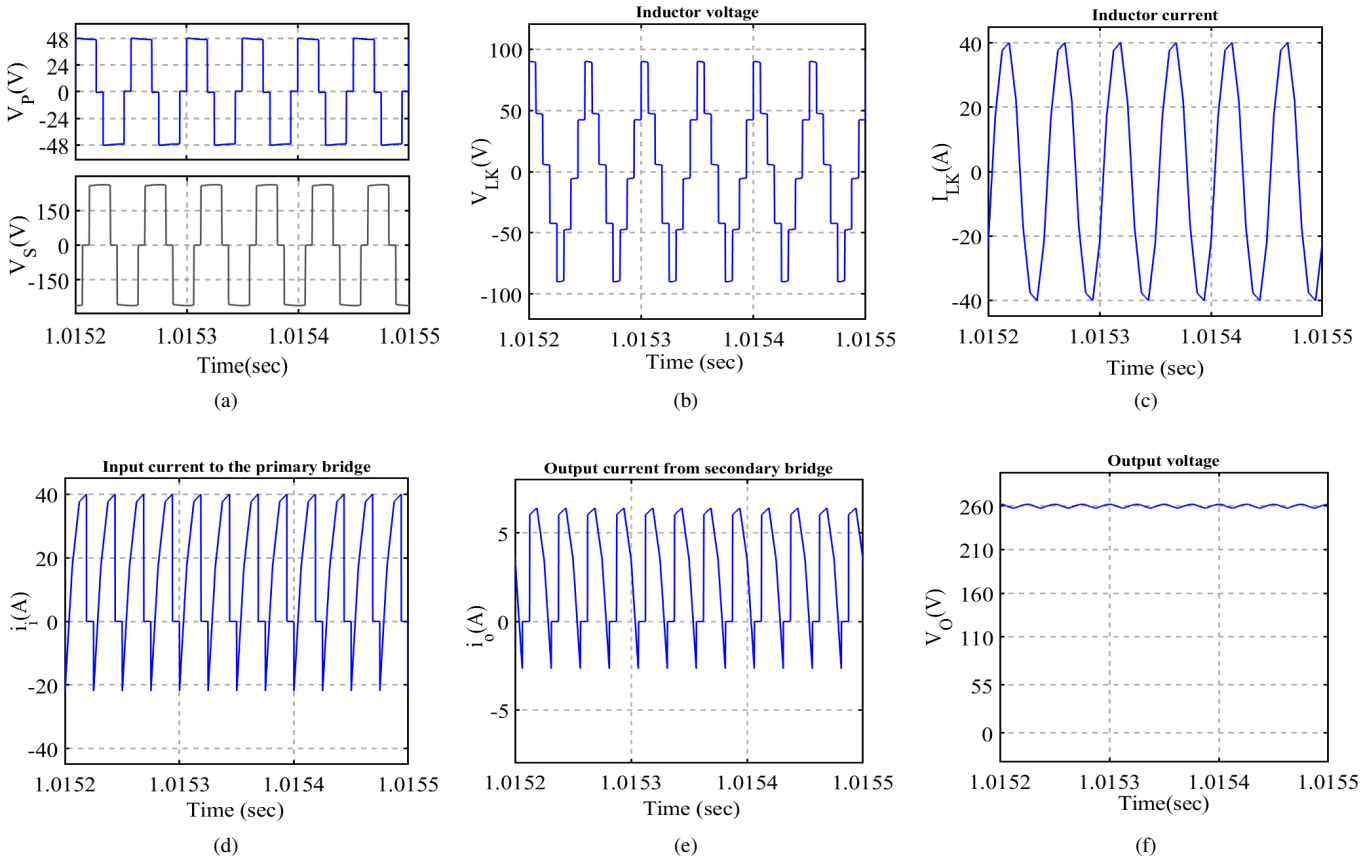

Fig. 7: Simulation results for DPS modulation (a) Primary and secondary voltage (b) Inductor voltage (c) Inductor current (d)Input current to the primary bridge (e) Output current from the secondary bridge (f) Output voltage

TABLE I: Simulation parameters

Parameter	Value
Power	1 kW
Input voltage (V_d)	48 V
Output voltage (V_O)	300 V
Switching frequency	20 kHz
Turns ratio of transformer	1:6.25
Leakage inductance of transformer	0.010 μH
External inductance	14.404 μH
Output capacitor	7.50 μF

the bridges having frequency twice the switching frequency as depicted in Fig. 6 (d) and (e) respectively. In Fig. 6 (f), output voltage of the converter is shown which is little less than the 300 V due to drop across the switches. Open loop results of SPS are in coherence with the theoretical results.

B. With DPS Modulation

The simulation results for the DPS modulation method are shown in Fig. 7. The external phase shift of 25% and inner phase shift of 62.5% with respect to the time period are taken for the simulation. The primary and secondary bridge voltages are shown in Fig. 7 (a). The ac side three-level inductor voltage and current are shown in Fig. 7 (b) and (c) respectively. The three-level voltage is due to the conduction of both switches of the same leg together and correspondingly the input and output current of bridges are zero as depicted in Fig. 7 (d) and (e). In this case also, the frequency of these currents are twice the switching frequency. The output voltage is reduced to 260 V approximately as given in Fig. 7 (f). The waveforms obtained are matching with the results present in the existing literature. The input and output power of the DAB converter for both SPS and DPS modulation schemes are shown in Fig. 8(a) and (b) respectively. The reduction in output power for boost mode of operation is due to the switching losses and can be minimized by employing ZVS operation.

IV. Conclusion

In this paper, a brief introduction about two modulation (i.e. SPS and DPS) techniques for the DAB converter along with the steady state operation for SPS scheme is presented. Various voltage and current waveforms of SPS scheme are in coherence with its theoretical steady-state results. The open loop simulation results for SPS and DPS modulation schemes are discussed in detail. In SPS modulation, primary and secondary voltages are two level and for DPS, it is three level. The frequency of both input and output current of the primary and secondary bridges are twice the switching frequency for

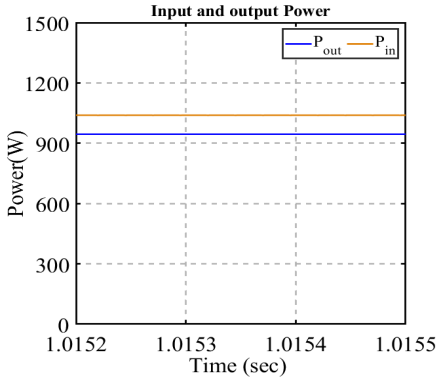

(a)

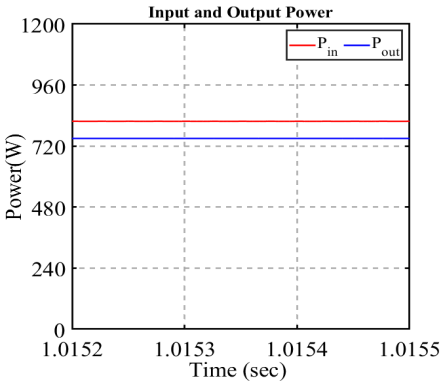

(b)

Fig. 8: Input and output power of DAB converter for both the modulation schemes (a) SPS (b) DPS

both the modulation techniques. The efficiency of the converter for both the modulation techniques are approximately equal to 90% which can be improved further by including soft switching operation. The DAB can be used for microgrid as well as EV applications utilizing the bidirectional power flow capability of the converter.

REFERENCES

[1] P. C. Loh, D. Li, Y. K. Chai, and F. Blaabjerg, "Hybrid ac–dc microgrids with energy storages and progressive energy flow tuning," *IEEE transactions on power electronics*, vol. 28, no. 4, pp. 1533–1543, 2012.

[2] P. He and A. Khaligh, "Comprehensive analyses and comparison of 1 kw isolated dc–dc converters for bidirectional ev charging systems," *IEEE Transactions on Transportation Electrification*, vol. 3, no. 1, pp. 147–156, 2016.

[3] B. Zhao, Q. Song, W. Liu, and Y. Sun, "Overview of dual-active-bridge isolated bidirectional dc–dc converter for high-frequency-link power-conversion system," *IEEE Transactions on power electronics*, vol. 29, no. 8, pp. 4091–4106, 2013.

[4] B. M. Kumar, A. Kumar, A. Bhat, and P. Agarwal, "Comparative study of dual active bridge isolated dc to dc converter with single phase shift and dual phase shift control techniques," in *2017 Recent Developments in Control, Automation & Power Engineering (RDCAPE)*. IEEE, 2017, pp. 453–458.

[5] I. Kayaalp, T. Demirdelen, T. Koroglu, M. U. Cuma, K. C. Bayindir, and M. Tumay, "Comparison of different phase-shift control methods at isolated bidirectional dc-dc converter," *International Journal of Applied Mathematics Electronics and Computers*, vol. 4, no. 3, pp. 68–73, 2016.

[6] G. Barone, G. Brusco, A. Burgio, M. Motta, D. Menniti, A. Pinnarelli, and N. Sorrentino, "A dual active bridge dc-dc converter for application in a smart user network," in *2014 Australasian Universities Power Engineering Conference (AUPEC)*. IEEE, 2014, pp. 1–5.

[7] D.-K. Jeong, H.-S. Kim, J.-W. Baek, J.-Y. Kim, and H.-J. Kim, "Dual active bridge converter for energy storage system in dc microgrid," in *2016 IEEE Transportation Electrification Conference and Expo, Asia-Pacific (ITEC Asia-Pacific)*. IEEE, 2016, pp. 152–156.

[8] L. Xue, Z. Shen, D. Boroyevich, P. Mattavelli, and D. Diaz, "Dual active bridge-based battery charger for plug-in hybrid electric vehicle with charging current containing low frequency ripple," *IEEE Transactions on Power Electronics*, vol. 30, no. 12, pp. 7299–7307, 2015.

[9] F.-M. Ni and T.-L. Lee, "Implementation of a bidirectional three-phase dual-active-bridge dc converter with hybrid modulation for electric vehicle applications," in *2014 International Conference on Intelligent Green Building and Smart Grid (IGBSG)*. IEEE, 2014, pp. 1–4.

[10] H. Qin and J. W. Kimball, "Closed-loop control of dc–dc dual-active-bridge converters driving single-phase inverters," *ieee transactions on power electronics*, vol. 29, no. 2, pp. 1006–1017, 2013.

[11] Y. Shi, R. Li, Y. Xue, and H. Li, "Optimized operation of current-fed dual active bridge dc–dc converter for pv applications," *IEEE Transactions on Industrial Electronics*, vol. 62, no. 11, pp. 6986–6995, 2015.

[12] A. Kumar, A. Bhat, and P. Agarwal, "Comparative analysis of dual active bridge isolated dc to dc converter with single phase shift and extended phase shift control techniques," in *2017 6th International Conference on Computer Applications In Electrical Engineering-Recent Advances (CERA)*. IEEE, 2017, pp. 397–402.

[13] V. Karthikeyan and R. Gupta, "Closed-loop control of isolated dual active bridge converter using dual phase shift modulation," in *IECON 2015-41st Annual Conference of the IEEE Industrial Electronics Society*. *IEEE*, 2015, pp. 002 800–002 805.

[14] D. Das and K. Basu, "Optimal design of a dual-active-bridge dc–dc converter," *IEEE Transactions on Industrial Electronics*, vol. 68, no. 12, pp. 12 034–12 045, 2020.

[15] A. R. R. Alonso, J. Sebastian, D. G. Lamar, M. M. Hernando, and A. Vazquez, "An overall study of a dual active bridge for bidirectional dc/dc conversion," in *2010 IEEE Energy Conversion Congress and Exposition*. IEEE, 2010, pp. 1129–1135.

[16] M. Kheraluwala, R. W. Gascoigne, D. M. Divan, and E. D. Baumann, "Performance characterization of a high-power dual active bridge dc-to-dc converter," *IEEE Transactions on industry applications*, vol. 28, no. 6, pp. 1294–1301, 1992.